# Bipolar resistive switching based on bis(8-hydroxyquinoline) cadmium complex: Mechanism and non-volatile memory application*

Wang Ying(王 颖), Yang Ting(杨 汀), Xie Ji-Peng(谢吉鹏), Lü Wen-Li(吕文理), Fan Guo-Ying(范国莹), and Liu Su(刘 肃)†

*Institute of Microelectronics, School of Physical Science and Technology, Lanzhou University, Lanzhou* 730000, *China*

(Received 21 October 2012; revised manuscript received 22 January 2013)

Stable and persistent bipolar resistive switching was observed in an organic diode with the structure of indium-tin oxide (ITO)/bis(8-hydroxyquinoline) cadmium ($Cdq_2$)/Al. Aggregate formation and electric field driven trapping and detrapping of charge carriers in the aggregate states that lie in the energy gap of the highest occupied molecular orbital (HOMO) and the lowest unoccupied molecular orbital (LUMO) of the organic molecule were proposed as the mechanism of the observed bipolar resistive switching, and this was solidly supported by the results of AFM investigations. Repeatedly set, read, and reset measurements demonstrated that the device is potentially applicable in non-volatile memories.

**Keywords:** resistive switching, memory, aggregation, bis(8-hydroxyquinoline) cadmium

**PACS:** 73.40.Sx, 84.37.+q, 73.61.Ph, 85.65.+h **DOI:** 10.1088/1674-1056/22/7/077308

## 1. Introduction

Since 1971, the unusual resistance switching effect has been observed in various inorganic[1–6] and organic materials under an electric field. The resistance switching effect in various device structures provides a variety of possible next-generation nonvolatile memory (NVM) applications. Generally, NVMs are studied with two switching behaviors: unipolar and bipolar switchings. The polarities of the external voltage for the reset and the set processes are identical in unipolar switching, while they are the opposite in bipolar switching.[7,8] The memory effect has been demonstrated in various device architectures, such as a single organic layer and multiple organic-inorganic layers sandwiched between two electrodes. Various kinds of organic materials are reported as the single layer in NVMs, such as small molecules,[9–15] conjugated polymers,[16–21] polymer blends,[22,23] copolymers,[24,25] polymer–metal nanopartical blended structures,[17,26,27] conjugated polymer–donor–acceptor blends,[28] and molecules embedded in a superamolecular matrix.[29] The typical organic multilayers used in resistive switching devices include the trilayers of organic molecules/metal nanoparticles/organic molecules,[9,30–32] organic molecules/core-shell nanoparticles/organic molecules,[33] and semiconducting molecules/insulating molecules/semiconducting molecules,[34] and the bilayers of inorganic salt/molecules[35] and metal oxides/polymers.[36]

Up to now, several mechanisms and models have been proposed to explain the resistive switching in different organic device architectures. The switching effect in devices based on a single polymer or molecule layer was attributed to the formation of conducting filaments.[9,16,18] The redox mechanism was considered to be the origin of the resistive switching in copolymer-based devices.[24] The formation of valence controlled charge transfer complexes was proposed as the mechanism in CuTCNQ (TCNQ=7,7,8,8-tetracyano-p-quinodimethane)-based NMVs.[12] The electric field induced charge transfer between organic molecules and metal nanoparticles was proposed to cause the switching effect in single layer devices based on organic–metal nanoparticle blends and trilayer devices with the structure of organic molecules/metal nanoparticles/organic molecules.[17,26,33] In addition, a charge trapping model,[15,32] electrode-induced two-dimensional single-electron tunneling,[37] the change of molecular orientation,[29] conjugation modifications by the reduction/oxidation of molecules,[38,39] the electrochemical process of ionic conduction,[14,40] and the electric field dependent depletion at the metal–organic interface[27] were proposed to cause the resistive switching in different devices.

In this paper, we report on the bipolar resistive switching effect and the memory characteristics of a single-layer sandwiched device using bis (8-hydroxyquinoline) cadmium ($Cdq_2$) as the active memory material. Stable and reproducible bipolar resistive switching is observed, and the non-volatile memory characteristic is demonstrated in organic diodes with the structure of indium tin oxide (ITO)/$Cdq_2$/Al. Aggregate formation and electric field driven trapping and detrapping of charge carriers in the aggregate states that lie in the energy gap between the highest occupied molecular orbital (HOMO) and the lowest unoccupied molecular orbital (LUMO) of the $Cdq_2$

*Project supported by the National Natural Science Foundation of China (Grant No. 10974074).

†Corresponding author. E-mail: liusu@lzu.edu.cn

© 2013 Chinese Physical Society and IOP Publishing Ltd 

molecule contribute to the observed bipolar resistive switching, which is supported by atomic force microscopy (AFM) investigation of the active organic films.

## 2. Experiment

The small molecule complex $Cdq_2$ was synthesized and purified according to a synthesis procedure similar to that of tris(8-hydroxyquinoline) aluminum.[41] The fundamental principle of the synthesis is to combine an 8-hydroxylquinoline anion with a $Cd^{2+}$ cation. Here, 0.001 mol cadmium sulphate was reacted with 0.002 mol 8-hydroxylquinoline at a temperature of 60–70 °C, and sodium hydroxide or ammonium acetate was used to adjust the pH value of the solution. The sample device with the structure shown in Fig. 1 was fabricated by vacuum depositing $Cdq_2$ on a pre-cleaned ITO coated glass substrate followed by vacuum depositing a thin aluminum film as the top electrode. The area of the device defined by a shadow mask was around 5 $mm^2$. The vacuum pressure for organic and electrode deposition was about $10^{-3}$ Pa. The current–voltage ($I$–$V$) characteristic was measured by a home-made automatic semiconductor device analyzer. All electrical measurements were conducted under ambient conditions without any encapsulation. The bias polarity was defined with reference to the top Al electrode.

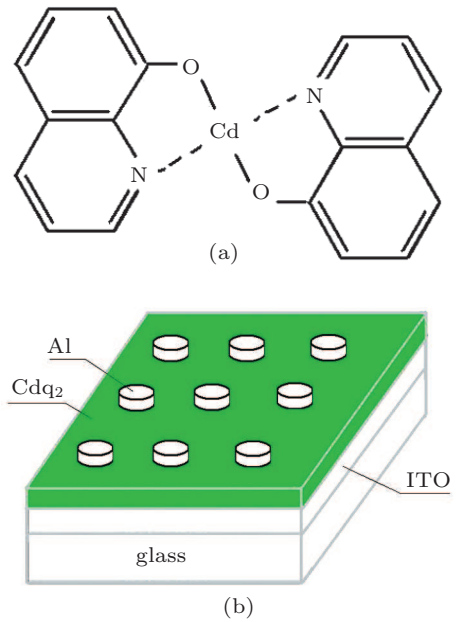



**Fig. 1.** (color online) (a) The molecular structure of $Cdq_2$, and (b) the structure of the resistive switching device based on $Cdq_2$.

## 3. Results and discussion

The resistive switching effect was observed in a forward–backward voltage-scan cycle, as shown in Fig. 2. The $I$–$V$ curve of the voltage sweep cycle starting from a negative voltage could be divided into six sections from (i) to (vi) (Fig. 2). When the forward voltage was scanned from −8.4 V to 1 V (section (i)), the $I$–$V$ curve exhibited a behavior similar to that of a reverse biased diode, and the resistance of the device in this voltage range was high. When the voltage ramped up from about 1 V to 4.9 V (section (ii)), the $I$–$V$ characteristic exhibited an Ohmic-like behavior, and the rate of current increase with voltage was larger than that in section (i). The corresponding resistance in section (ii) was therefore lower than that in section (i). When the voltage was further increased from 4.9 V to 9 V, the rate of current increase slowed down to around zero. When the voltage swept backwards from 9 V to −1 V (section (iv)), the current decreased, and the $I$–$V$ curve exhibited a behavior similar to that of a positively biased diode. The $I$–$V$ curve exhibited another Ohmic-like behavior with a resistance close to that in section (ii) as the voltage swept from about −1 V to −4.9 V (section (v)). When the voltage decreased further, a remarkable negative difference resistance (NDR) appeared (section (vi)), that is, the current decreased with the increase in voltage.

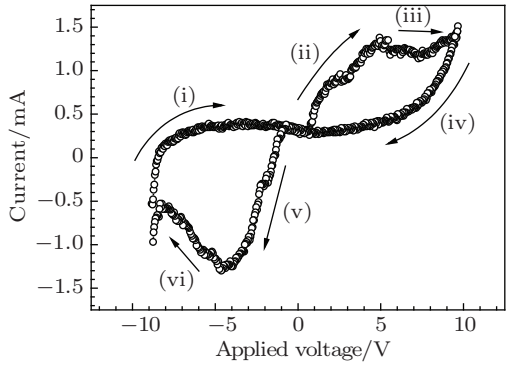



**Fig. 2.** The current–voltage characteristic taken by forward and backward voltage scans, and three successive cycles of forward and backward voltage scans.

The sections in the voltage scans and the assignment of resistance states to logical values are summarized in Table 1. Switching between the high resistance state (HRS) and the low resistance state (LRS) of the device was performed numerous times. The device was repeatedly set, read, and reset in air, as demonstrated in Fig. 3. To write "0", that is, the reset of the device, a voltage of +7.8 V was applied, which set the device in HRS. In the subsequent reading process, a voltage of 2.9 V was applied, which corresponded to the scan process of section (iv) in Fig. 2. As the device was in HRS, a small current of $2.8\times10^{-4}$ A was measured. To write "1", that is, the set of the device, a voltage of −7.0 V was applied, which corresponded to the voltage scan of section (vi) and set the device in LRS. A subsequent application of the voltage of 2.9 V read out the resistance state, which corresponded to the voltage scan of section (ii) in Fig. 2. As the device was in LRS, a large current of $9.7\times10^{-4}$ A was measured.

**Table 1.** The sections in the voltage scans, the resistance states, and the assignment of logical values.

| Voltage scan/V | Section (i) −8.4→1.0 | Section (ii) 1.0→4.9 | Section (iii) 4.9→9.0 | Section (iv) 9.0→−1.0 | Section (v) −1.0→−4.9 | Section (vi) −4.9→−8.4 |
|---|---|---|---|---|---|---|
| Resistance state | HRS | LRS | HRS | HRS | LRS | LRS |
| Logic value | 0 | 1 | 0 | 0 | 1 | 1 |

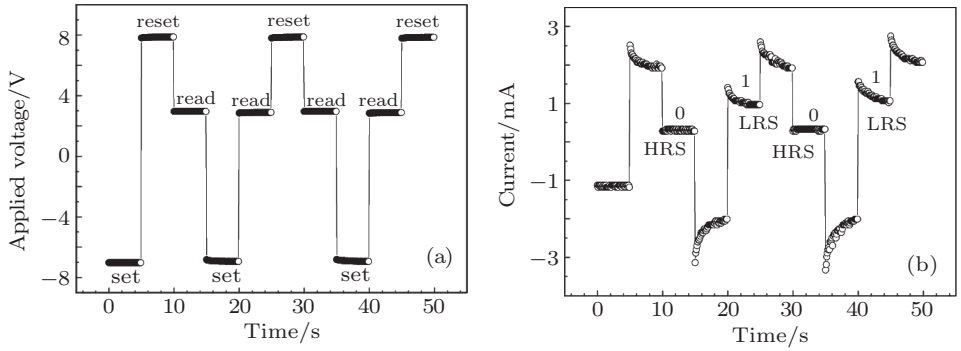



**Fig. 3.** The typical set, reset, and read cycles of the ITO/$Cdq_2$/Al device. (a) Applied voltage pulse with set, reset, and read voltages of −7.0 V, 7.8 V, and 2.9 V, respectively; (b) current response. The low and high resistance states are assigned to the logic of "1" and "0", respectively.

In order to clarify the switching mechanism, we studied the surface morphology of the $Cdq_2$ film on the ITO glass substrate using atomic force microscopy. It can be seen from Fig. 4 that particles with sizes of 0.1 μm to 1 μm, which can be regarded as molecular aggregates, are uniformly scattered in the film. Molecular aggregates are mesomorphous structures, which means that the degree of molecule order is between the crystal and the amorphous. In contrast to most crystals and nanocrystals in which energy states for the free motion of electrons exist, and to most amorphous structures in which electrons are localized to monomolecules, aggregates have electrons that are delocalized within only several molecules. Each orbital of a monomolecule splits into several orbitals with different energies through the coupling in the aggregate. These new energy states are called aggregate states. Some of the aggregate states lie in the energy gap between the HOMO and the LUMO of the monomolecule,[42] and thus act as trap states for electrons. Based on the above observations and considerations, we propose that the observed resistive switching and NDR are due to the aggregate formation in the $Cdq_2$ film. The aggregate states in the HOMO–LUMO gap of the $Cdq_2$ molecule serve as traps for either electrons or holes. Electric field driven trapping and detrapping of charge carriers in these trap states cause the resistive switching and NDR of the device. In fact, the formation of aggregate states was demonstrated to be the cause of negative difference resistance in a 3,4,9,10-perylentetracarbonsäuredianhydrid (PTCDA)-based organic diode.[42] The trapped charge in aggregates alternates the distribution of the electric field that is parallel to the normal of the metal–organic interface in the case of the film with a pure amorphous structure, which results in the three-dimensional motion of charge carriers in the organic film as shown in Fig. 5.

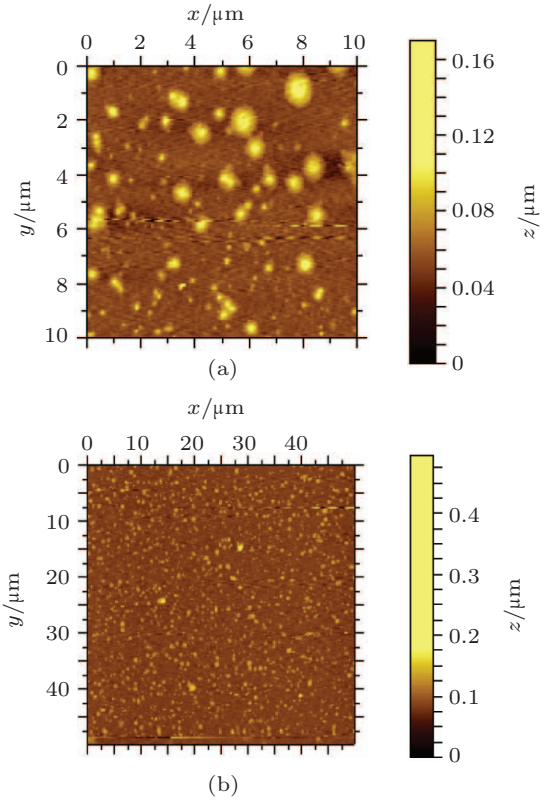



**Fig. 4.** (color online) AFM images of $Cdq_2$ film on ITO glass substrate with sizes of (a) 10 μm×10 μm and (b) 50 μm×50 μm.

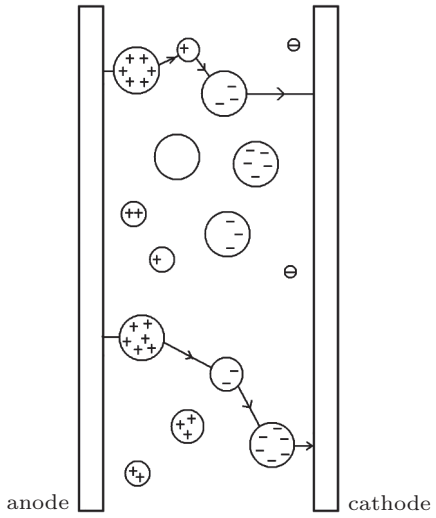



**Fig. 5.** Schematic diagram of the three-dimensional current path in the organic film caused by trapped charge in the aggregates in the case of a positive voltage bias.

The $I$–$V$ characteristic shown in Fig. 2 belongs to a more general bipolar resistive switching characteristic, as shown in Fig. 6.[43,44] We explain the detailed mechanism of such a switching characteristics with the help of the energy diagram in Fig. 7. Generally, as mentioned above, aggregate states exist in the energy gap of LUMO and HOMO, which serve as either electron or hole traps. For simplicity, these aggregate states are approximated hereafter as single-level electron or hole traps, as shown in Fig. 7. The trap states in as-prepared devices without bias are assumed to be unoccupied. At the beginning of the forward scan starting from a large negative field, $F_a$, the effective depths of electron and hole traps are small, as schematically illustrated in Fig. 7(a), therefore the number of trapped holes and electrons is small. As $|F|$ decreases, the effective depths of the traps increase, and so does the number of trapped electrons and holes. The current of the device is limited by the metal–organic contacts, and the $I$–$V$ curve exhibits a diode-like behavior. It should be noted that under a negative bias, electrons (holes) are injected from the anode (cathode) into the organic. At $F = F_0$, the number of trapped holes and electrons reaches maximum, and so do the number of trapped electrons near the anode and those of trapped holes near the cathode. In the forward field scan of section (ii), on one side, the Schottky barrier for electrons at the cathode–organic interface, $\varphi_{ec}$, and that for holes at the anode–organic interface, $\varphi_{ha}$, are largely reduced by the trapped holes near the cathode and the trapped electrons near the anode, respectively. On the other side, the effective depths of the traps become smaller and smaller, and the trapped electrons and holes are released continuously. These released carriers make an additional contribution to the device current, which is denoted as $j_{RC}$. The device current $j$ can be expressed as $j = j_{am} + j_{RC}$, where $j_{am}$ denotes the current density of the device whose organic film is free of aggregates, that is, ideal amorphous, and $j_{RC}$ denotes the current contribution from the carriers released from the traps. As the number of released carriers is large, and the electrode contacts are nearly Ohmic, the $I$–$V$ curve exhibits an Ohmic-like behavior. In the forward scan of section (iii), most of the trapped electrons and holes are released, and the number of released free carriers decreases with time due to the recombination and extraction by the electrodes, and thus their contribution to the device current, $j_{RC}$, decreases and finally becomes zero at $F = F_1$. Meanwhile $j_{am}$ increases due to the increased field. The decrease in $j_{RC}$ and the increase in $j_{am}$ with increasing field lead to the device current first decreasing and then increasing with increasing field. During the backward field scan of $F_b \to -F_0$ (section (iv)), on one side, the electron and hole traps become deeper and deeper, and thus more and more free carriers are trapped; and on the other side, the Schottky barrier for electrons at the cathode–organic interface, $\varphi_{ec}$, and that for holes at the anode–organic interface, $\varphi_{ha}$, are increased due to the fact that electrons are trapped near the cathode and holes are trapped near the anode. The filling of the traps is completed at $F = -F_0$. As no carriers are released from the traps during the scan, the device current is $j = j_{am} + j_{RC} \approx j_{am}$, that is the $I$–$V$ characteristic is diode-like. For the backward scan from $F_0$ to $-F_{th}$ (section (v)), on one side, the effective trap depths decrease, while the detrapped electrons and holes increase; and on the other side, the energy barrier for electrons at the anode, $\varphi_{ea}$, is so largely reduced by the trapped holes there that it can no longer effectively limit the electron injection at the anode. The same changes occur for the hole energy barrier, $\varphi_{hc}$, and the hole injection at the cathode. Therefore, $j \approx j_{RC}$, and the $I$–$V$ curve is nearly Ohmic. At $F = -F_{th}$, the density of the released carriers reaches a maximum, which results in a maximum of the device current. For the backward scan of $-F_{th} \to -F_a$ (section (vi)), the number of free carriers decreases due to the decreased release rate of trapped carriers compared with the recombination and extraction by the electrodes. The device current is governed by detrapped charge conduction and injected carrier conduction in the field range from $-F_{th}$ to $-F_1$, while only the injected carriers contribute to the current in the field range from $-F_1$ to $-F_a$.

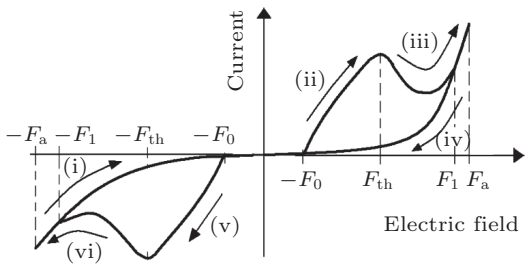



**Fig. 6.** The general current–voltage characteristics of bipolar resistive switching. The field scan sections (i) $-F_a \to F_0$, (ii) $F_0 \to F_{th}$, and (iii) $F_{th} \to F_b$ are forward scan; while sections (iv) $F_b \to -F_0$, (v) $-F_0 \to -F_{th}$, and (vi) $-F_{th} \to -F_a$ are backward scan.

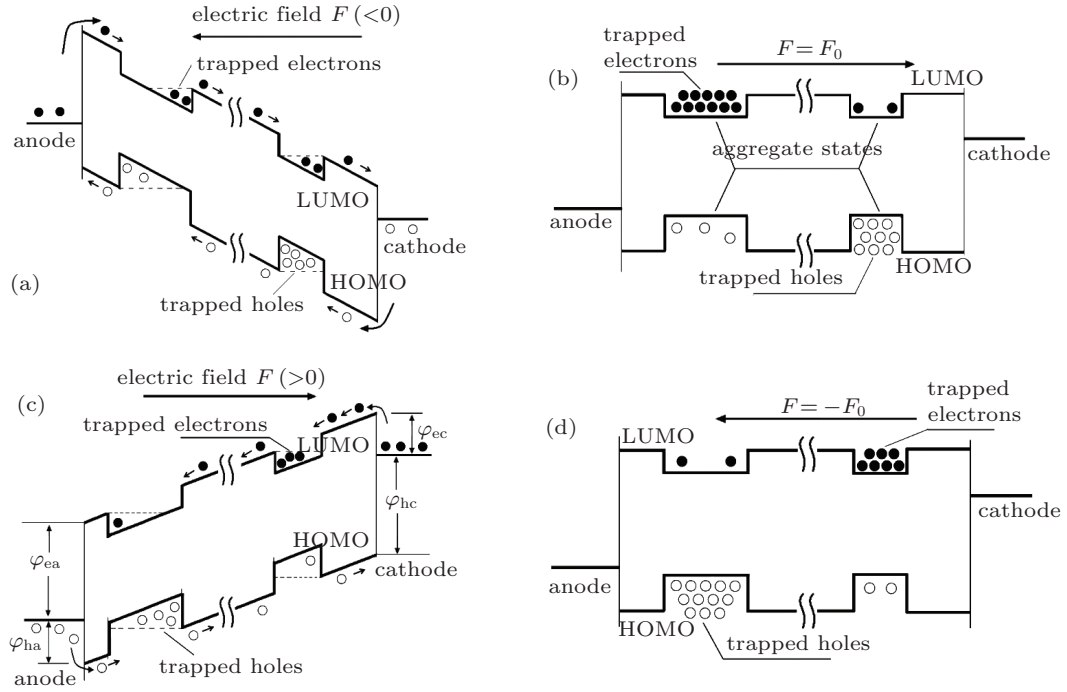



**Fig. 7.** Schematic diagrams of the energy levels and trapped carriers in aggregates during different regions of the field scan: (a) $-F_a \rightarrow F_0$, forward scan of section (i); (b) $F = +F_0$, end of forward scan of section (i); (c) $F_b \rightarrow F_0$, backward scan of section (iv); (d) $F = -F_0$, end of backward scan of section (iv).

## 4. Conclusion

In summary, we investigated the $I$–$V$ characteristics of a device with an ITO/$Cdq_2$/Al structure, in which stable and persistent bipolar resistive switching and NDR were observed, and a non-volatile memory characteristic was demonstrated. Aggregate formation and electric field driven trapping and detrapping of charge carriers in the aggregate states that lie between the HOMO and LUMO of the organic molecule were proposed as the mechanism of the resistive switching. AFM investigation showed that large particles formed by the aggregation of $Cdq_2$ molecules were uniformly scattered in the active film, which gave solid support for the proposed mechanism.

## References


[1] Panda D, Dhar A and Ray S K 2010 *J. Appl. Phys.* **108** 104513

[2] Zhang X T, Yu Q X, Yao Y P and Li X G 2010 *Appl. Phys. Lett.* **97** 222117

[3] Zhong W X, Chen X, Wu N J and Ignatiev A 2011 *Chin. Phys. B* **20** 097703

[4] Zhao J W, Liu F J, Huang H Q, Hu Z F and Zhang X Q 2012 *Chin. Phys. B* **21** 065201

[5] Li Y T, Long S B, Lü H B, Liu Q, Wang Q, Wang Y, Zhang S, Lian W T, Liu S and Liu M 2011 *Chin. Phys. B* **20** 017305

[6] Meng Y, Zhang P J, Liu Z Y, Liao Z L, Pan X Y, Liang X J, Zhao H W and Chen D M 2010 *Chin. Phys. B* **19** 037304

[7] Rolfe N, Desai P, Shakya P, Kreouzis T and Gillin W P 2008 *J. Appl. Phys.* **104** 083703

[8] Lee S, Kim H, Park J and Tong K J 2010 *J. Appl. Phys.* **108** 076101

[9] Tondelier D, Lmimouni K, Vuillaumea D, Fery C and Haas G 2004 *Appl. Phys. Lett.* **85** 5763

[10] Shi J P, Wen Z C, Song C A and Peng Y Q 2005 *Chin. J. Semicond.* **26** 1979

[11] Chen J S and Ma D G 2005 *Appl. Phys. Lett.* **87** 023505

[12] Potember R S, Poehler T O and Cowan D O 1979 *Appl. Phys. Lett.* **34** 405

[13] Li X S, Peng Y Q, Song C A, Yang Q S, Zhao M, Yuan J T and Wang H 2008 *Chin. J. Vacuum Sci. Techn.* **28** 394

[14] Müller R, Genoe J and Heremans P 2009 *Appl. Phys. Lett.* **95** 133509

[15] Lin J and Ma D G 2009 *Organic Electronics* **10** 275

[16] Chen Y C, Su Y K, Yu H C, Huang C Y and Huang T S 2011 *Appl. Phys. Lett.* **99** 143308

[17] Ouyang J Y, Chu C W, Szmanda C R, Ma L P and Y Y 2004 *Nature Materials* **3** 918

[18] Xu X J, Li L D, Liu B and Zou Y P 2011 *Appl. Phys. Lett.* **98** 063303

[19] Lauters M, McCarthy B, Sarid D and Jabbour G E 2006 *Appl. Phys. Lett.* **89** 013507

[20] Liu G, Zhuang X D, Chen Y, Zhang B, Zhu J H, Zhu C X, Neoh K G and Kang E T 2009 *Appl. Phys. Lett.* **95** 253301

[21] Kim T W, Oh S H, Lee J, Choi H, Wang G, Park J, Kim D Y, Hwang H and Lee T 2010 *Organic Electronics* **11** 109

[22] Liu X H, Ji Z Y, Tu D Y, Shang L W, Liu J, Liu M and Xie C Q 2009 *Organic Electronics* **10** 1191

[23] Moeller S, Forrest S R, Perlov C, Jackson W and Taussig C 2003 *J. Appl. Phys.* **94** 7811

[24] Ling Q D, Song Y, Ding S J, Zhu C X, Chan D S H, Kwong D L, Kang E T and Neoh K G 2005 *Adv. Mater.* **17** 455

[25] Song Y, Tan Y P, Teo E Y H, Zhu C X, Chan D S H, Ling Q D, Neoh K G and Kang E T 2006 *J. Appl. Phys.* **100** 084508

[26] Prakash A, Ouyang J Y, Lin J L and Yang Y 2006 *J. Appl. Phys.* **100** 054309

[27] Lai P Y and Chen J S 2009 *Organic Electronics* **10** 1590

[28] Chu C W, Ouyang J Y, Tseng J H and Yang Y 2005 *Adv. Mater.* **17** 1440

[29] Bandyopadhyay A and Pal A J 2004 *Appl. Phys. Lett.* **84** 999

[30] Ma L P, Liu J and Yang Y 2002 *Appl. Phys. Lett.* **80** 2997

[31] Ma L P, Pyo S, Ouyang J Y, Xu Q F and Yang Y 2003 *Appl. Phys. Lett.* **82** 1419

[32] Bozano L D, Kean B W, Deline V R, Salem J R and Scott J C 2004 *Appl. Phys. Lett.* **84** 607
[33] Reddy V S, Karak S and Dhar A 2009 *Appl. Phys. Lett.* **94** 173304
[34] Li Y, Qiu D F, Cao L Q, Shao C X, Pan L J, Pu L, Xu J Band Shi Y 2010 *Appl. Phys. Lett.* **96** 133303
[35] Ma L P, Xu Q F and Yang Y 2004 *Appl. Phys. Lett.* **84** 4908
[36] Verbakel F, Meskers S C J, Janssen R A J, Gomes H L, Cölle M, Büchel M and de Leeuw D M 2007 *Appl. Phys. Lett.* **91** 192103
[37] Tang W, Shi H Z, Xu Gu, Ong B S, Popovic Z D, Deng J, Zhao J and Rao G 2005 *Adv. Mater.* **17** 2307
[38] Li Q, Surthi S, Mathur G, Gowda S, Misra V, Sorenson T A, Tenent R C, Kuhr W G, Tamaru S, Lindsey J S, Liu Z M and Bocian D F 2003 *Appl. Phys. Lett.* **83** 198
[39] Bandyopadhyay A and Pal A J 2003 *Appl. Phys. Lett.* **82** 1215
[40] Sim R, Chan M Y, Wong A S W and Lee P S 2011 *Organic Electronics* **12** 185
[41] Li H, Zhang F J, Wang Y Y and Zheng D S 2003 *Mater. Sci. Engin. B* **100** 40
[42] Xie X N, Wang J Z, Loh K P and Wee A T S 2009 *Appl. Phys. Lett.* **95** 203302
[43] Scott J C and Bozano L D 2007 *Adv. Mater.* **19** 1452
[44] Yang Y, Ouyang J Y, Ma L P, Tseng R J H and Chu C W 2006 *Adv. Funct. Mater.* **16** 1001